Ultrasonic Resonance Approach to Measure Rolling Element Bearing Raceway Films In-Situ: A Practical Approach

W. Gray*, R. S. Dwyer-Joyce

The Leonardo Centre for Tribology, The University of Sheffield, Sheffield, United Kingdom, S32 3ZA

Keywords: Oil lubrication, Bearing, Starvation, In-situ measurement

Abstract

The lubricant film adhering to a bearing raceway is the primary contributor to developing an adequate inlet meniscus to avoid starvation and thus premature wear. This paper shows that lubricant films adhering to the raceways of rolling element bearings are measurable via an in-situ ultrasonic resonance technique, that is applicable to fully metallic bearings. This work first validates the measurement of free-surface oil films on bearing steel using the ultrasonic resonance method before applying to a fully metallic, cylindrical roller bearing. Practical considerations are discussed to optimise the measurement range and accuracy, and limitations are highlighted. Quantifying a dynamic raceway film into single thickness measurements is discussed, and two oils with a magnitude difference in viscosity are compared.

1 Introduction

Rolling element bearing contacts operate within the elastohydrodynamic (EHL) regime (1), and an exhaustive literature has developed studying the EHL film thickness (2, 3). Much of the early EHL work was completed by Dowson et al. (4, 5, 6, 7, 8, 9, 10) who developed equations to model EHL central and minimum film thickness, and assess how parameters such as load, speed, oil viscosity, bearing materials and inlet fill affect these film heights. It is known that the EHL inlet conditions, in particular the viscosity and quantity of lubricant available, are the primary governors of contact conditions (11, 12).

In classical EHL theory, it is assumed a contact always has ample lubricant supply, and therefore is fully flooded (9). However, this has been shown an inaccurate assumption in single contacts (13, 9, 14) and in full operating bearings with modified transparent raceways which allow the oil distribution to be monitored (15, 16). This finite inlet volume of oil, if inadequate, will lead to starvation. The authors here define starvation as the reduction in EHL central film thickness, when compared with the theoretical value, due to a lack of lubricant supply at the inlet. Grease lubricated bearings are known to operate for the majority of their lifetime under starved conditions (17, 18).

Within a rolling element bearing the inlet film to a contact is made up of that adhering to the ball/roller and that adhering to the raceway, as shown in Fig. 1. The distance from the contact centre to where these two films meet is the inlet meniscus, denoted as s. The roller film is determined by the rupture ratio at the outlet from the previous contact. When in pure rolling, there is a 50-50 split of the oil film onto the roller and raceway at the outlet (19, 20). However, EHL films are typically sub-micron, meaning so too is the roller film. Thus, the majority of the inlet film is fed by the lubricant adhering to the raceway surface.

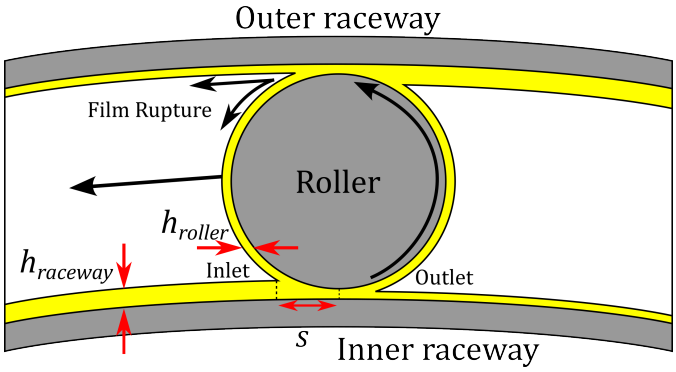

Figure 1: Schematic of the raceway and roller films joining to form the inlet meniscus to a rolling element bearing contact.

Damiens et al. (21) investigated starvation in elliptical contacts experimentally, analytically and numerically, based on the work of Elrod (22), Moes (23) and Chevalier et al. (14). Findings showed that oil side leakage was reduced with increasing ellipticity, suggesting that bearing form (ball, cylindrical, spherical) can have different lubrication phenomenon.

Numerous studies have controlled contact starvation through altering the thickness of the oil film entering a contact, which essentially models the raceway film (14, 21, 22, 24, 25, 26, 27). van Zoelen et al. (28) investigated oil distribution on a deconstructed raceway film without rollers, and found that distribution altered between bearing types when investigating both tapered and spherical raceways, with non-symmetrical distributions.

Chen et al. (15) and Chennaoui et al. (16) observed raceway distribution, but again on modified bearings. All of these works are optical in nature which limits them to a laboratory. Pramod et al. (29) used a modified capacitance method to calculate the inlet meniscus position, again which is governed by raceway films. Although, this method is aimed at measuring contact films, with an inlet condition change being a cause, not the measured effect. There are currently no other published techniques for measuring/assessing raceway thickness within metallic bearings that would be suitable for a laboratory or field setting.

In the last two decades ultrasonic sensors have been gaining momentum as an alternative technology to measure bearing lubricant conditions (30, 31, 32). This is due largely to their low cost, simplicity, and ability to propagate waves through solid and liquid media, meaning direct contact access is not required, enabling true in-situ measurements.

Ultrasonic reflections from thin films, that is a film thinner the ultrasonic wavelength, are enriched with information on the film thickness. Bearing contact measurements are difficult due to the spatial resolution of the sensors which means the Hertzian contact zone being smaller than the measurement area (33, 34).

However, the film adhering to the raceway, which makes up the majority of the inlet meniscus, is a much larger target, greater than the spatial resolution of ultrasonic sensors on larger bearings. When an oil film is within the magnitude of a quarter of the ultrasonic wavelength, destructive interference within the film causes a resonance phenomenon, the frequency of which, if measured, relates to the film thickness. The fundamentals of this resonance approach were conduced by Haines et al. (35) and Pialucha et al. (36, 37).

The resonance approach has been used to measure plate coatings (38, 39, 40), journal bearing thick films (41, 42, 43, 44), condensing water films (45, 46) and laboratory based surface films (47). There are three perquisites for the measurement of an intermediary layer thickness (i) the layer is within the resonant frequency range (typically 50μm to 500μm depending on the frequency of the sensor) and two given by Pedersen et al. (45); (ii) the layer has a significantly different acoustic impedance to both boundary media (iii) the layer is of planar thickness over the measurement area.

In previous work by the authors of this paper (48), ultrasonic sensors were successfully used to measure inner raceway lubricant thickness of an NU2244 bearing in-situ, using a acoustic resonance approach. This proved that the layer fully met the criteria (i) and (ii) and that the raceway films were stable enough that resonant frequencies were still detectable. This paper builds upon the previous work by fully validating the measurement of surface films by acoustic resonance methods on bearing like materials, exploring the practical post-processing limitations of the method, and developing a way to quantify raceway film thickness in-situ, across the rolling axis, allowing lubricant distribution leading into a contact to be appreciated.

2 Experimental Test Equipment

2.1 Cylindrical Bearing Test Rig

Fig. 2 shows the bespoke cylindrical roller bearing (CRB) test rig used for this work. A detailed description can be found by Howard (33) who developed the rig for his thesis. The rig houses a shaft mounted NU2244 cylindrical roller bearing, which is representative of a CRB that supports a low speed shaft in a $2.5\text{MW} - 3\text{MW}$ wind turbine gearbox. The bearing has a bore diameter of 220mm, a mean diameter of 310mm and has fifteen cylindrical rollers of 54mm diameter and 82mm length. During testing the inner raceway remains stationary, the outer raceway being belt driven up to a maximum of 100 revolutions-per-minute (rpm). This setup is to specifically test a bearing within a wind turbine epicyclic gearbox which operates in this manner. However, the measurement technique presented in this work is applicable outside of the wind turbine industry, and there is no detrimental impact of this setup as the necessary bearing rotation is still present.

A hall effect sensor monitored the rotation of the outer raceway of the test bearing whilst a purely radial load was applied to the shaft via two linkages. Load cells within each linkage gave load feedback. A single k-type thermocouple was bonded on the inner bore of the inner raceway, at a position next to the central ultrasonic sensor. Only one thermocouple could be used due to space restrictions limiting cable access. This sensor was used to determine the in-situ lubricant temperature for acoustic-velocity calculation.

During oil testing a hydraulic pump fed lubricant between the raceways, at 60° from the bottom-dead-centre. A scavenger pump was used to collect and recirculate this oil feed so that the bearing had a constant lubricant supply. A pressure transducer in the inlet to the oil pump ensured there was lubricant flow during testing. The load, rotational speed and oil pump were all controlled through a LabVIEW interface.

The rig design intention was for the bottom, heavy loaded region to be flooded with oil to provide advantageous lubrication conditions for the contacts in this region. In actuality, as the rollers rotate they wade through the oil creating wedges, and recirculation is still needed from the outlet of one roller contact to the inlet of the next. The effect is more pronounced at higher bearing speeds and it means fully flooded conditions cannot be assumed. However, some level of beneficial side-flow can be assumed to be present.

As the inner raceway remains stationary, this raceway was chosen for instrumentation to simplify the cabling. Fig. 3a shows an array of ultrasonic sensors along the inner bore of the inner raceway of the test bearing. Sensors were a bespoke instrumentation made of 'bare' piezoelectric ceramics cabled and potted, as described in the authors previous work (48). By having seven sensors, the

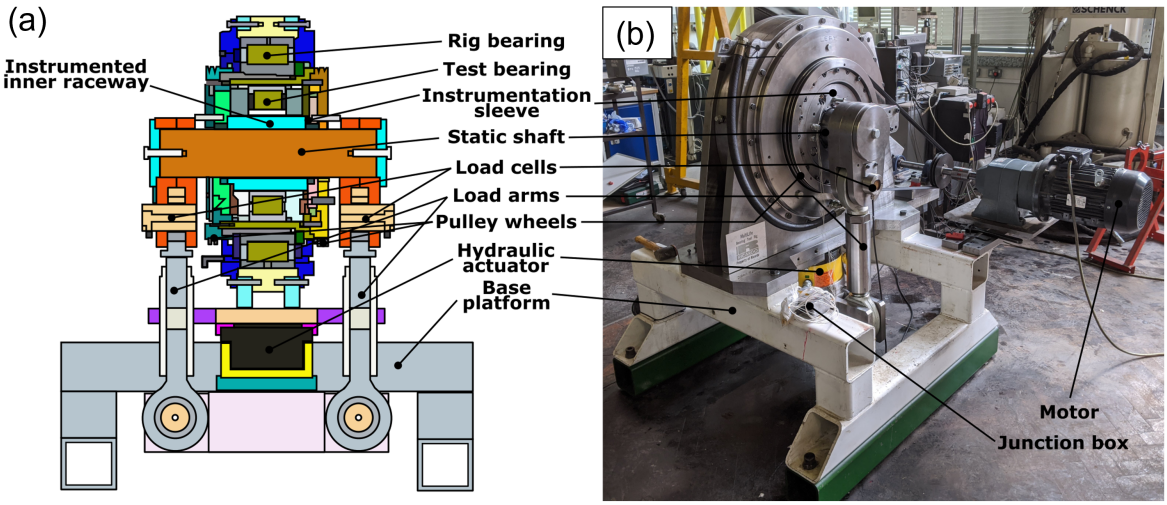

Figure 2: Cylindrical roller bearing test rig (a) schematic (b) photograph, taken from (34).

film could be monitored at discrete points along the rolling axis. More sensors could not be included due to cable space limitations.

Fig. 3b shows the ultrasonic pulser-receiver (UPR) system used to take the ultrasonic measurements. The UPR was used to both excite sensors and record the data enriched reflections in a pulse-echo format. A digitiser and buffer were used to digitally store the reflections. Control of the ultrasonic UPR system was done using a LabVIEW interface. The UPR excited sensors sequentially at a rate of 9kHz per channel. As the pulse rate is so high it is assumed a near instantaneous measurement across all active sensors. The digitiser sampled reflections at a rate of 100MHz.

A series of short 10s tests were completed. These were performed from unloaded to 600kN of pure radial load applied in steps of $100kN$, and at speeds of 20rpm to 100rpm in 20rpm increments. Incorporating the bearing size, this calculates as $6,200\text{nd}_\text{m}$ to $31,000\text{nd}_\text{m}$.

2.2 The KOVOT Rig

The Known Oil Volume Test Rig (KOVOT) was developed to validate the ultrasonic resonance method of free surface oil films. The purpose of the rig is to perform as an extremely well dimensioned oil bath, of a theoretically known volume. When a lubricant, of known density and volume, is deposited into the bath, the film thickness can be calculated from the dimensions of the rig. The layer thickness can then be measured using ultrasound, and the resonance approach validated against the known thickness. Additionally, a wet film comb gauge can be used as an extra measurement method. Fig. 4 shows a schematical representation of the KOVOT, and the raceway film it is intended to model.

Six ultrasonic sensors were instrumented to the underside of the base plate, as shown in Fig. 4. Four were at 90° separations, and two were located at the plate centre. When the oil layer was stabilised, so long as the plate was accurately levelled, the readings from all locations should be the same. These were controlled to take ultrasonic measurements of the oil film using a Picoscope-Optmux ultrasonic pulser-receiver data acquisition kit, controlled via a LabVIEW interface on a laptop personal computer. Red T symbols represent k-type thermocouples which were present to monitor temperature during testing.

The intention of the rig was to simulate resonances in lubricants on a bearing raceway. The base plate, upon which the oil layer sits and through which ultrasonic waves travel, was manufactured from EN31 bearing steel, heat treated to $795HV20$ with just a 1.27% hardness difference from the NU2244 bearing. The base plate thickness, a crucial dimension as it determines the set path length of the ultrasonic signal, was measured as $t_{plate} = 19.50\text{mm} \pm 0.007\text{mm}$, and therefore agreeable with the raceway tolerance. The roughness of the lubricant face side of the test plate was investigated using an optical InfiniteFocus SL Alicona, and measured as mean $Ra = 0.287\mu\text{m} \pm 0.020\mu\text{m}$. To ensure the levelness of the test plate during testing, a CG60 Cromwell Circular Level, bullseye style gauge was used in combination with a digital a Laseriner MasterLevel Box Pro. The base was deemed level when perpendicular axis readings of 0.00° were achieved.

During tests ultrasonic readings where taken during film thinning and of the stabilised layer. Once the lubricant film had stabilised, the theoretical film thickness was calculated from a simple volume by area equation:

$$h_\theta = V/A \tag{1}$$

where V is volume in $\text{m}^3 = \text{ml} \times 10^{-6}$ and A is area calculated as $A = \pi D^2/4$. When the oil film had been allowed

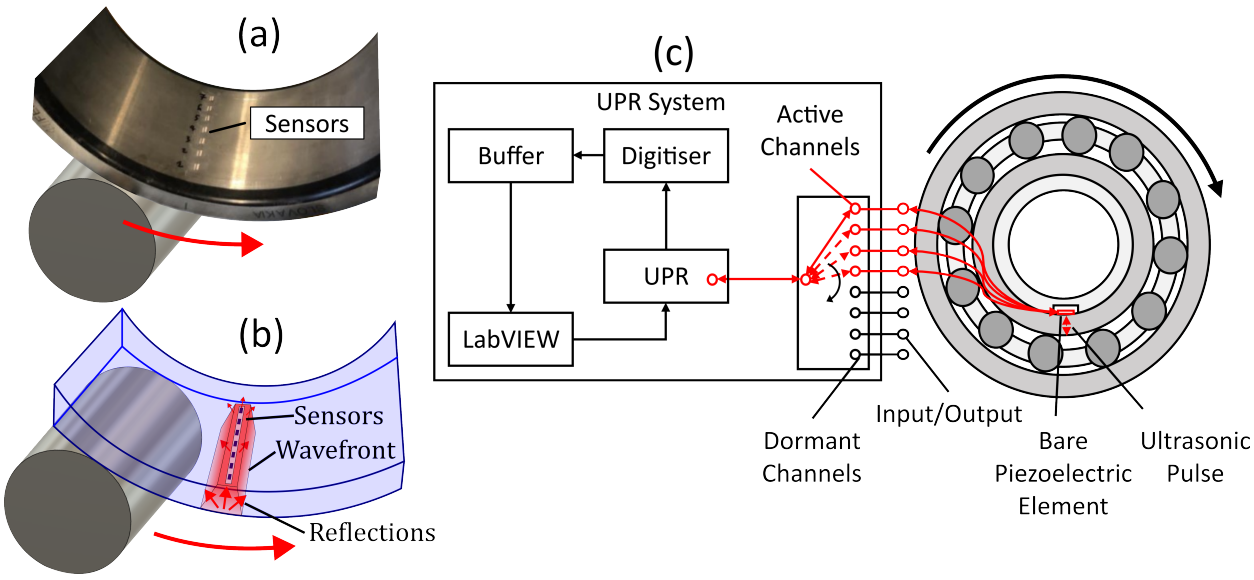

Figure 3: (a) & (b) Roller bearing inner raceway with a row of ultrasonic piezo elements instrumented on the inner, non-contact face (c) Schematic of ultrasonic pulser-receiver linked with instrumented bearings, adapted from (33).

to fully stabilise, the film height could also be assessed using a wet film comb gauge, as shown in Fig. 5. The film height is measured as the average between the last wet tooth and first dry tooth. Fig. 5c shows schematically a reading of $262.5\mu\text{m} \pm 12.5\mu\text{m}$.

2.3 Lubricant Properties

Three oils were used in this work. The *VWR Avantor calibration oil 85095.260* (85095.260) is a standard low viscosity calibration oil used, used for the bench top experimental work. *Hyspin VG32* (VG32) and *Alpha SP 320* (VG320) are machine oils with an order of magnitude difference in viscosity. Key parameters are shown in Table 1. The acoustic velocity relationship was determined through measuring the time-of-flight of an ultrasonic signal over an oven controlled temperature ramp, as described in (49).

3 The Ultrasonic Resonance Technique

The measurement of lubricant films within rolling element bearings inlet region is discussed by the authors Gray & Dwyer-Joyce (48) in which a detailed explanation of the ultrasonic principle is applied. Here, a brief summary of that explanation will be given and built upon.

The acoustic impedance z of a material, a product of its density ρ and acoustic velocity c, signifies the ability of mechanical wave to transmit. Materials with low z values suffer from high attenuation, and so wave amplitudes quickly diminish. When a wave strikes a boundary between two materials with different acoustic impedances, part of the wave is transmitted and part is reflected. Equation 2 determines the reflection coefficient R, which is the proportion of wave amplitude reflected when compared with the initial wave amplitude.

$$R = \frac{z_2 - z_1}{z_2 + z_1} \tag{2}$$

Subscripts 1 and 2 denote the materials either side of the boundary. The greater the mismatch the more reflection occurs, for example between steel ($z_{steel} \approx 4.7 \times 10^7 \text{kg/m}^2\text{s}$) and air ($z_{air} \approx 0.4 \times 10^3 \text{kg/m}^2\text{s}$) a majority of wave energy would be reflected, $R_{steel-air} = 0.9999872 \approx 1$. However, Equation 2 assumes material bodies long enough that the wave can fully form and propagate. When boundaries exist close together, within a proximity less than an ultrasonic wavelength, waves overlap and the individual boundaries act as a single point of reflection. The reflected wave is then a summation of the constructive and destructive wave interferences between boundaries. Fig. 6a shows a two-boundary system of a solid steel layer, an oil layer and an air layer.

The p_i, p_r and p_t represent the incident, reflected and transmitted pressure waves respectively. The p_a wave represents the wave transmitted from the steel-oil boundary and p_b the wave reflected from the oil-air boundary. Kinsler et al. (50) explains that transmitted and incident waves across a boundary are always in phase regardless of acoustic impedances at a boundary. Also, when a wave travelling through an acoustically soft material reaches the boundary with an acoustically harder material $z_1 < z_2$ the reflected portion of the wave is still perfectly in phase with the incident wave. However, when $z_1 > z_2$ the reflected wave is 180°out of phase with the incident wave. Referring to Fig. 6a, as there is an impedance gradient as $z_1 > z_2 > z_3$, the p_a and p_b waves are inherently 180°out of phase. However, this phase change is also dependent on the distance between the steel-oil and oil-air boundaries i.e. the thickness of the middle layer. Because of the phase difference causing destructive interference of waves

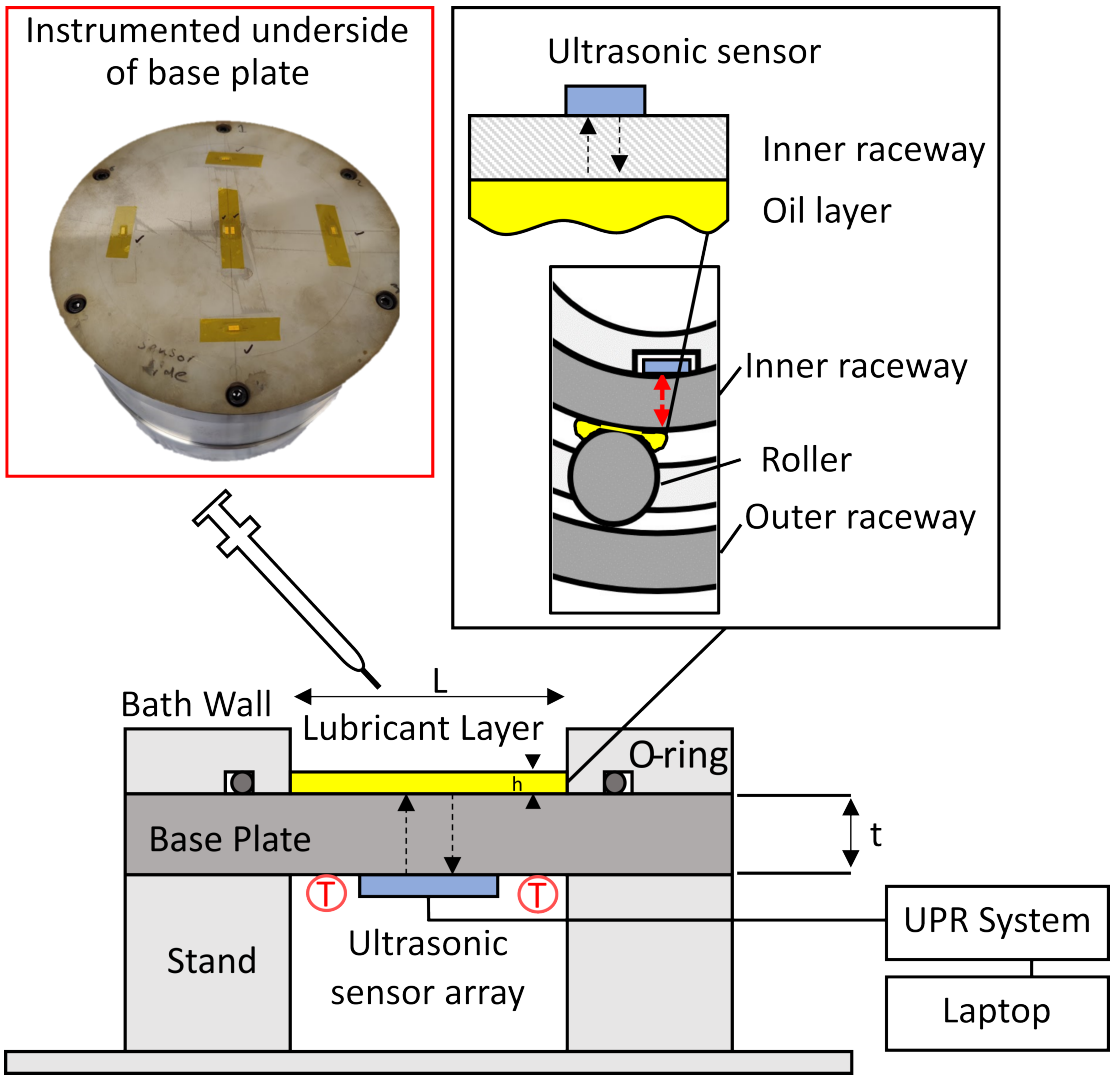

Figure 4: Schematic of the KOVOT rig, and the model representation of a lubricated raceway. The red T symbols show where thermocouples are temporarily bonded during testing. A picture of the instrumented underside of the base plate is also shown.

within the middle layer, Haines et al. (35) showed that when $z_1 > z_2 > z_3$ the middle layer resonates at odd integer multiples of the fundamental frequency (f_0, $3f_0$, $5f_0$, etc.). The case of the complex reflection coefficient from a dual-boundary as in Fig. 6a, in terms of pressure, was given by (51):

$$R = \frac{R_{23} + R_{23}^{(2i\alpha_2 h)}}{1 + R_{12}R_{23}^{(2i\alpha_2 h)}} \tag{3}$$

where R_{12} and R_{23} are the reflection coefficients at the first and second media boundaries. α_2 is a coefficient referring to the second medium, defined as:

$$\alpha_2 = k_2 + i\beta \tag{4}$$

where β is the attenuation coefficient and c_2 is the wave velocity through the middle layer, k_2 is the wave number calculated as:

$$k_2 = \frac{2\pi f}{c_2} \tag{5}$$

where f is frequency and c_2 is acoustic velocity in the second medium. Although Equation 3 is complex, incorporating amplitude and phase, Haines et al. (35) gave an equation for the real, amplitude portion:

$$|R| = \left[\frac{(R_{23} + R_{12}e^{-2\beta h})^2 - 4R_{12}R_{23}e^{-2\beta h}\sin^2 k_2 h}{(1 + R_{12}R_{23}e^{-2\beta h})^2 - 4R_{12}R_{23}e^{-2\beta h}\sin^2 k_2 h}\right]^{1/2} \tag{6}$$

Fig. 6b shows the modelled real amplitude portion of the reflection coefficient calculated from Equation 6 for four different oil film thicknesses. The resonant frequencies are calculated by the following:

$$(2n+1)f_0 = \frac{(2n+1)c_2}{4h} \tag{7}$$

where n is any integer value ($n = 0, 1, 2, 3, \dots$). At these particular frequencies, p_a and p_b interfere to create a short duration standing wave, greatly reducing the amplitude of p_r. This is then observed by a drop in the reflection coeffi-

Table 1: Lubricant properties.

Oil	Viscosity at 40 °C, cSt	Viscosity at 40 °C, cSt	Acoustic Velocity, m/s
85095.260	2.9	2.4	1502.6-2.7817T
VG32	32	5.3	1531.3-3.4270T
VG320	328	24	1576.3-2.9586T

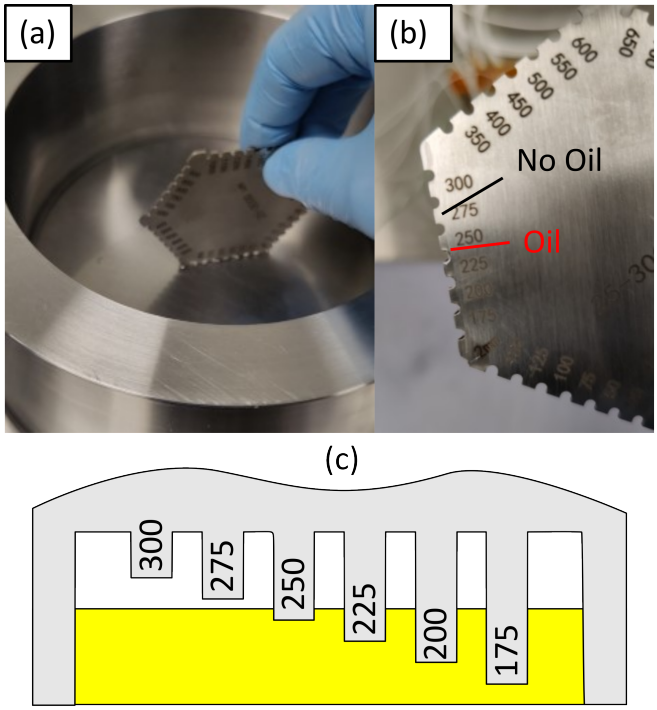

Figure 5: a & b show pictures of the comb gauge being dipped into a stationary oil layer. Oil is present on the 250μm tooth but not the 275μm tooth, giving a reading of 262.5μm$\pm$12.5μm. A schematic representation is given in c.

cient. The first of these resonances is the fundamental frequency, f_0. To find the relationship between fundamental frequency f_0 and film thickness, Equation 5 is used with $f = f_o$, multiplied by the thickness of the middle body h, and equalled to the phase change when $n = 0$:

$$\begin{aligned} k_2 h &= (2n+1)\frac{\pi}{2} \\ \therefore \frac{2\pi f_o h}{c_2} &= \frac{\pi}{2} \end{aligned} \tag{8}$$

And so:

$$h = \frac{c_2}{4 f_o} \tag{9}$$

Swapping c_2 for terms in the general wave equation $c = \lambda f$ into Equation 9 shows that the middle layer resonates at its fundamental frequency when its thickness is a quarter of that of the ultrasonic wave:

$$h = \frac{\lambda}{4} \tag{10}$$

This resonance occurring in media at a quarter of the interacting wavelength is seen in other wave interactions, such as coupling piezoelectric elements to water and air (52), and coupling ultrasonic matching-layers with metals in ultrasonic viscometers (53).

Equation 9 shows that $h \propto 1/f_o$ and so the thicker films have smaller fundamental frequencies and thinner films have larger fundamental frequencies. This is shown in Fig. 6b, which compares model data of films between 1μm and 200μm. The 1μm film shows no detectable reduction in R across the presented frequency spectrum, demonstrating that there is a lower limitation of the resonance method. In reality, a resonance would occur if the layer could be excited by a high enough frequency, but an increased frequency leads to more attenuation, and thus a diminishing reflection amplitude.

The 20μm fundamental frequency occurs at $\approx$ 18.75MHz. The thicker films have lower fundamental frequencies; for the 200μm film $f_0 \approx 1.8$MHz, and further resonant dips are seen within the shown frequency spectrum at approximately 5.4, 9, 12.6MHz which are the higher order odd harmonics. For a metal-lubricant-air contact, resonances occur at odd integer multiples of the fundamental frequency due to the acoustic impedance gradient of the materials.

When practically measuring resonant frequencies, it can be difficult knowing which harmonic is detected if only one dip is present within the sensor bandwidth. However, if multiple resonances are detected, knowing the frequency difference is $\Delta f = 2f_0$ between harmonics, the following relationship can be made where $\overline{\Delta f}$ is the mean measured frequency difference between dips:

$$h = \frac{c_2}{2\overline{\Delta f}} \tag{11}$$

This can be a much more practical measurement approach, especially with a limited frequency bandwidth.

3.1 Acoustic Velocity Calibration

Equations 9 and 11 show that the thickness measurement is dependent not only on the measured f_0 value, but also on the acoustic velocity through the lubricant which can be altered by stress fields (54, 55), temperature (56, 57, 43, 48) and potentially degradation via a change of bulk modulus or from inclusion of debris particles affecting the homogeneity of the lubricant.

For all tests run in this work fresh, non-degraded lubricants were used as surface-films, meaning they are unconstrained and therefore unstressed. Consequently, the acoustic velocity-temperature relationship is what governs the change in the speed of sound. With an increase in oil temperature, there is a decrease in the speed of sound.

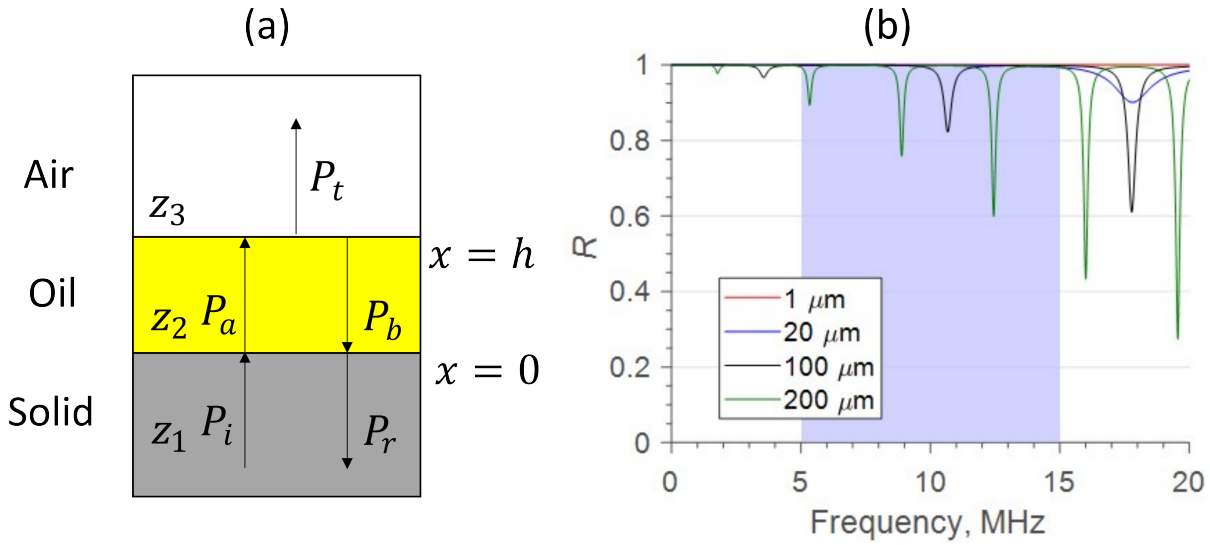

Figure 6: a) Adapted from (48) (a) Schematic of free surface film b) Model of free surface film resonance response at different layer thicknesses. The blue shaded region highlights a typical usable −6db bandwidth of a 10MHz central frequency piezo.

This has been shown to be very repeatable, and linear in natural oils (56, 57), and a very similar relationship is seen in synthetic oil, as seen for example by Beamish (43).

To determine the acoustic velocity of lubricants, a bespoke ultrasonic test rig was used. The measurement principle was to take ultrasonic time-of-flight measurements across a well defined chamber length full of oil, whilst the lubricant underwent a reverse temperature ramp. Thermocouples monitored the lubricant and ambient temperature. Acoustic velocity was calculated by dividing the distance of wave travel by the time of reflection return, and plotted against temperature to determine the acoustic velocity-temperature relationship. Rig calibration was performed using a distilled water test, of which the acoustic velocity-temperature relationship is very well documented (58, 59). The determined relationship of acoustic velocity to temperature for the oils used in this work are shown in Table 1, in the form:

$$c = y + xT$$

Where c is acoustic velocity in m/s, y is the y-intercept in degrees °C, x is the velocity-temperature gradient in $\mathrm{m \cdot s^{-1} \cdot {}^{\circ}C^{-1}}$, and T is the temperature of the oil in degrees °C.

4 Signal Processing Considerations

When measuring resonance phenomenon, the reflection coefficient is calculated from recorded signals as:

$$R = \frac{A_{mes}(f)}{A_{ref}(f)} \tag{12}$$

Where $A(f)$ refers to the Fast Fourier Transform (FFT) amplitude and subscripts *ref* and *mes* refer to a reference steel-air reflection and free-surface oil film reflection signal respectively, taken during testing. More detail about fundamental signal capture and data processing is given in the authors previous work (48). For this work, a live modal reference was generated from reflections of the raceway-air boundary, between roller passes.

4.1 Reflection Time Duration

The measurement range of the resonance approach is influenced with post-processing operations. Before transferring a time-domain signal into the frequency domain, a user decision must be made on the duration of reflection on which to analyse. Fig. 7 shows a typical ultrasonic reflection, divided into three sections: the nose, the body and the tail:

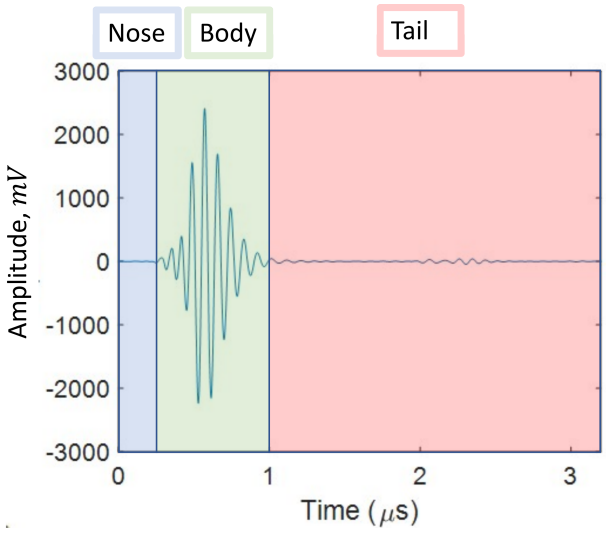

Figure 7: Different sections of a typical ultrasonic reflection.

Nose Section before the actual signal starts which does not contain any film data as it is the recording before the wave hits the sensor face. However, it must be distinguishable from the body of the wave, to eliminate signal cropping.

Body The reflection body is the main portion of the signal, which is similar to a classic sinusoidal wave, and this region contains the majority of the film thickness data within the signal. In the vast majority of all ultrasonic post processing, it is the body of the signal which is used.

Tail The tail of the signal proceeds the body, but is less a defined length, and more an area where oscillations in the signal are clear, but have amplitudes orders of magnitude smaller than those of the body.

Fig. 8 compares thickness measurements of an n10 calibration oil droplet landing and then spreading on an aluminium plate, taken using the ultrasonic resonance approach from a sensor mounted on the underside of the plate, and thus not in contact with the oil. During the test, the oil droplet thinned and thus the resonant frequency of the layer increased. The analysed reflection duration was altered in the time domain by clipping data from the reflection tail before performing performing an FFT and then completing the resonance analysis. The four measurements given are therefore all from a single recorded data set.

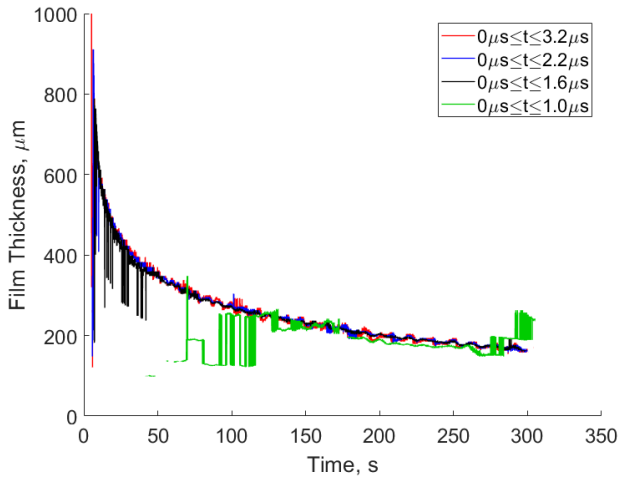

Figure 8: Thickness measurements of a spreading oil droplet, taken using the resonance approach, of a single data set, with varying reflection durations. Adapted from (48).

The longest reflection analysed was $0 \leq t \leq 3.2\mu$s shown in red, where t is the analysed reflection time. This incorporates a large tail and had the largest measurement range. The shortest was $0 \leq t \leq 1\mu$s shown in green, which ignores all of the tail and only incorporates the nose and body in post-processing.

Results show that as the tail of the signal is clipped, shortening the capture window, the measurement sensitivity to thicker films at the start of the test is lost, but the signal is still sensitive to the thinner films below $\lesssim 250\mu$m. The longest reflection analysed ($0 \leq t \leq 3.2\mu$s) gives the most stable film measurement across the entire thickness spectrum of the test. Therefore, the result suggests the signal tail contains resonance information relating to thicker films. Measurement sensitivity is related to the number of resonating echoes (60). By reducing the signal duration in post-processing, the echo number is synthetically reduced, hindering measurement sensitivity, and so the measurement range is reduced. This result suggests the measurement range of the resonance approach can be finitely improved upon by increasing the duration of signal capture.

4.2 Usable Bandwidth for Resonance Measurements

Fig. 9a shows the first 30MHz of the frequency spectrum of an example in-situ resonance bearing measurement. Two large dips in R occur at 5MHz (green) and 15MHz (yellow), near the transition regions between frequency lobes, which are governed by the central frequency of the piezo element and the pulse width applied. If there is some form of general decrease or lateral frequency shift in the FFT amplitude of the measurement reflection, due to sensor age, temperature, pressure or some other effect, these two points will naturally show a drop in R, but not due to resonance, and therefore these points determine the absolute frequency boundaries of resonance analysis.

The defined bandwidth should be constrained between these two frequencies, and outside of this bandwidth the signal is unusable due to its susceptibility to noise influence. This is clear from the spectral plot shown in Fig. 9b, generated from stacking multiple resonance spectra over time, which shows straight bands of noise above and below these transition frequencies, but within is a resonant frequency pattern indicative of a raceway film, as discussed in the authors previous work (48).

For the in-situ tests a conservative $-6db$ bandwidth was applied, highlighted in the blue region of Fig. 9a, within which there are clear dips in R to ≈ 0.95 due to the presence of an oil film. The dip amplitudes are more subtle than the resonances seen within the validation tests. This reduction in amplitude is theorised to be due to more beam spread due to the curved nature of the raceway, the use of a live modal-reference as opposed to an air reference, and the relatively thick raceway films that are measured, which are towards the upper limit for the resonance approach.

4.3 Rules to Determine the Order of a Single Resonant Dip

When using the resonant measurement method, it is beneficial to measure at least two dips. Doing so reduces drift error that may occur from measuring a dynamic film, as discussed by Chen (46) and in the thesis by Gray (49), and

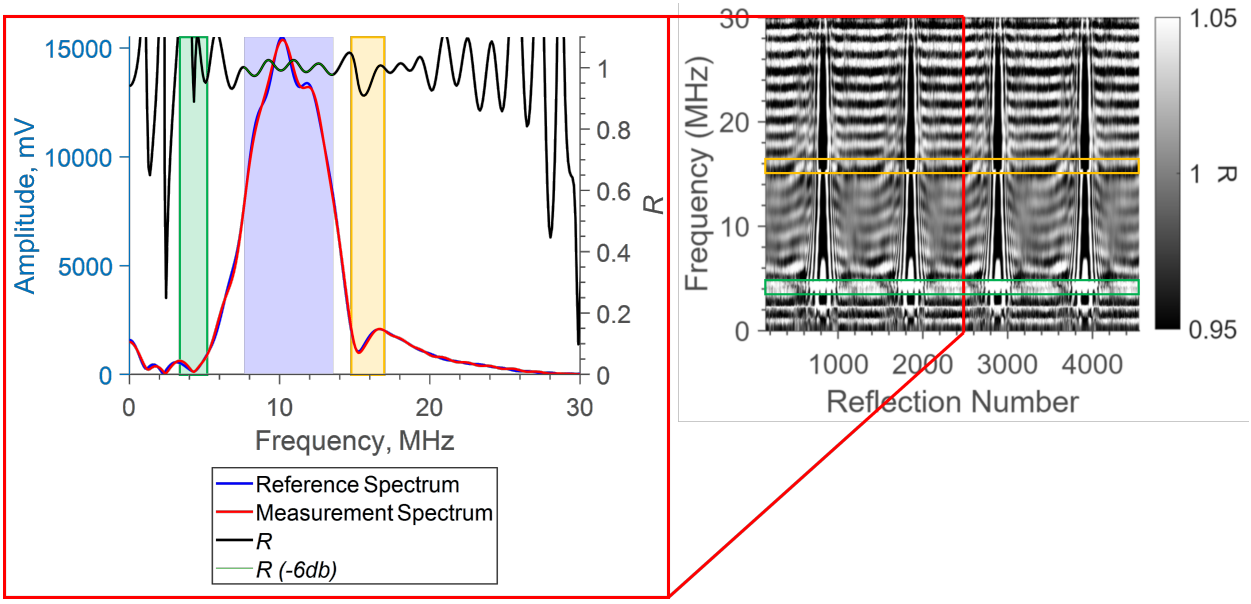

Figure 9: Example resonance plot from an in-situ raceway film measurement. Shown is the FFT plots of the reference and measurement signal, and from this the calculated reflection coefficient. Also shown is a spectral plot with a moving resonance pattern within the bandwidth, indicative of a present raceway lubricating film.

if only a single resonant dip is measured, there can be ambiguity regarding whether it is the resonant frequency or a higher order harmonic leading to potential measurement inaccuracies (48).

In Fig. 6 the blue zone represents a typical −6db bandwidth (BW). Take for example the 100μm film, where only the higher order $3f_0$ is detected within this bandwidth. Incorrectly identifying $3f_0$ as f_0 is the biggest threat to using a single resonance dip, and if this occurs the calculated film thickness will be out by a factor of more than 2.

Three independent rules are presented in Table 2, the first two of which were previously determined by Gray & Dwyer-Joyce (48), to assess whether a single resonance f_r is in fact the fundamental frequency.

If any of the conditions in Table 2 are met, the bandwidth is deemed large enough to detect other odd harmonics and therefore if not present it is assumed $f_r = f_0$. However, if the conditions cannot be satisfied, the assumption cannot be made, and at least 2 resonances must be recorded and $\overline{\Delta f}$ calculated and used in Equation 11 to make a thickness calculation. The rules in Table 2 are applicable to a free surface film only. For trapped film analysis, where resonances do not occur at just odd harmonics, an altered analysis approach is required.

5 Ultrasonic Resonance Method Precision

As Equation 9 shows, measurement precision is governed by the fundamental frequency of the film, and the acoustic velocity through the lubricant, which is in turn governed primarily by temperature when referring to raceway films. Fig. 10 is taken from Gray & Dwyer-Joyce where the coloured bars represent the measurement error for a given resonant frequency.

Fig. 10a shows an increasing resonant frequency with a reducing film thickness for the VG320 oil with a conservative −6db bandwidth applied. Measurement error reduces with increasing f_0 as the fixed frequency precision becomes a smaller percentage of the measured f_0. Using Equation 11, the minimum detectable film is 141μm at 20 °C and 119μm at 100 °C. This discrepancy is due to the change in acoustic velocity with a temperature change. A thicker film corresponds with a lower fundamental frequency and therefore tightly banded resonances. Thus, the frequency discretisation determines the upper limit of measurable film thickness. This plot will look similar for most oils and greases as the speed of sound value is a similar magnitude across all grades tested.

Fig. 10b shows that the measurement error and measurement thickness limitation can both be improved upon by increasing the measurement precision within the frequency domain, either via improved hardware or up to a point, zero-padding (61).

6 Validation of the Resonance Method

When using the KOVOT rig to validate the resonance method, *VWR Avantor calibration oil 85095.260* was used which has a viscosity $\nu = 4.4$cSt at 20 °C, and was found to flow across the entire plate surface and stabilise within 1 hour. Four different volumes of oil were used for the validation tests; 4ml, 5ml, 6ml and 7ml which should form theoretical film thicknesses of 264μm, 283μm, 339μm and 396μm respectively, if the layer formed is perfectly stable and level. Before applying the oil, a thin layer of Polysorbate 80, a non-ionic surfactant, was rubbed onto the plate surface to improve the surface wettability.

Table 2: Bandwidth rules to determine appropriate use of a single resonant frequency.

Rule	Reasoning
$f_r \leq \frac{BW_{max}-BW_{min}}{2}$	If a single resonance is detected, and is assumed as $3f_0$, the rule determines a bandwidth range adequate to detect either f_0 or $5f_0$ above or below f_r respectively. If this condition is met and only a single resonance is present then $f_r = f_0$.
$\frac{f_r}{3} \geq BW_{min}$	If the bandwidth minimum is less than a third of the frequency of the detected resonance, and only one resonance is detected, then it is confirmed that the detected frequency is not a higher order harmonic and thus $f_r = f_0$.
$\frac{f_r}{3} \times 5 \leq BW_{max}$	This rule suggests a single resonance measured is $3f_0$, and from this calculates the fundamental frequency and thus suggests where $5f_o$ will occur in the bandwidth. Then, if BW_{max} is greater than this predicted $5f_0$ frequency, and no resonance is present, the single resonance is proven to not be $3f_0$ and must instead be f_0.

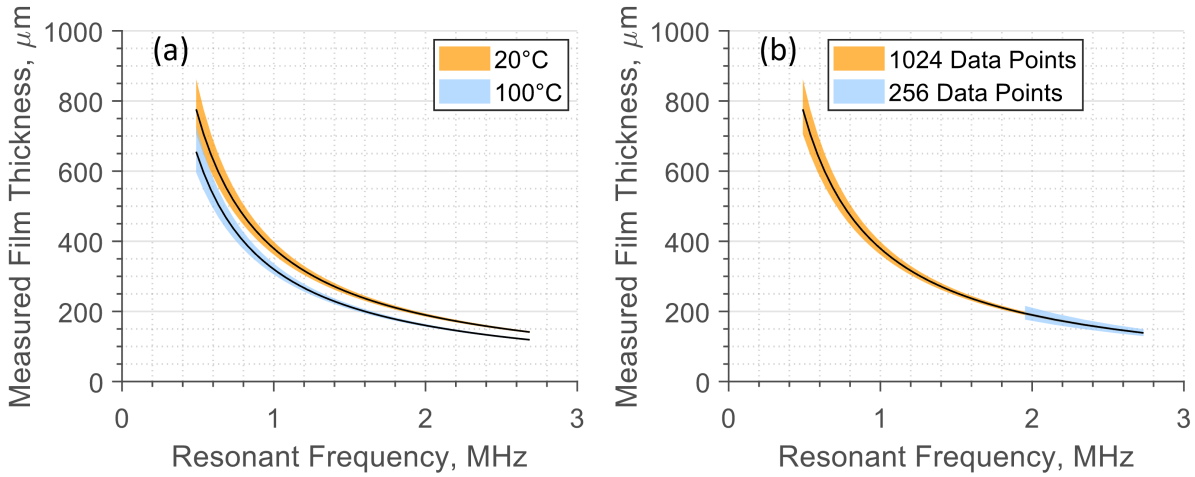

Figure 10: Comparison of theoretical measurable thickness and interval with an increasing fundamental resonant frequency, with (a) two temperature extremes (b) different levels of signal padding at $20°C$, adapted from Gray & Dwyer-Joyce (48).

During the oil thinning, the film resonance was monitored on a single sensor located at the plate centre, over a 60 minute duration. Fig. 11, formed by stacking individual R vs. frequency plots to form time and frequency axes, where R is plot intensity, shows a spectral analysis of the thinning oil layers, with the contrast limited to the theoretical $R \leq 1$. There are clear bands of resonance due to oil film presence, and the frequency of these resonance increases over time with oil spread due to the inversely proportional relationship between fundamental frequency and film thickness.

At the start of each test, there is an initial parched period where $R = 1$ at all frequencies as there is no oil present, and so the wave is fully reflected from the steel-air interface. The oil is then applied and initially the film is relatively thick, meaning f_0 is low, and the higher order harmonic fringes are tightly packed in the frequency axis.

As an oil spread, the fundamental frequency increased, as did the frequency between harmonics. Towards the end of the test the oil layer had spread over the entirety of the plate, forming a stable film, which is why the frequency differences between resonances become fixed and parallel for a short duration before the test end.

As the deposition volume increased, the time taken to achieve a stable layer, defined by the resonant fringes becoming parallel, shortened as a larger oil volume can cover the test plate quicker and thus achieve stability sooner. The final frequency difference between resonant fringes at the end of each test is related to the thickness of the stabilised layer. Larger oil deposits formed thicker films and thus resonant fringes that were more tightly banded.

Interestingly, thinner films are observed to have resonances of lower R values. This is shown by the decrease in R of resonances in one test as the film thins, and also between the stabilised layers of decreasing oil volume deposits. For the 7ml case the stabilised resonant amplitude $R \approx 0.5$. However, for the 4ml case $R \approx 0.2$. Dou et al. (60) showed that as echo number reduces, so too does the magnitude of the resonance amplitude. With thicker films, the signal attenuates more, thus reducing the potential number of echoes recorded and so the minima is reduced. This is not observed when using Equation 6

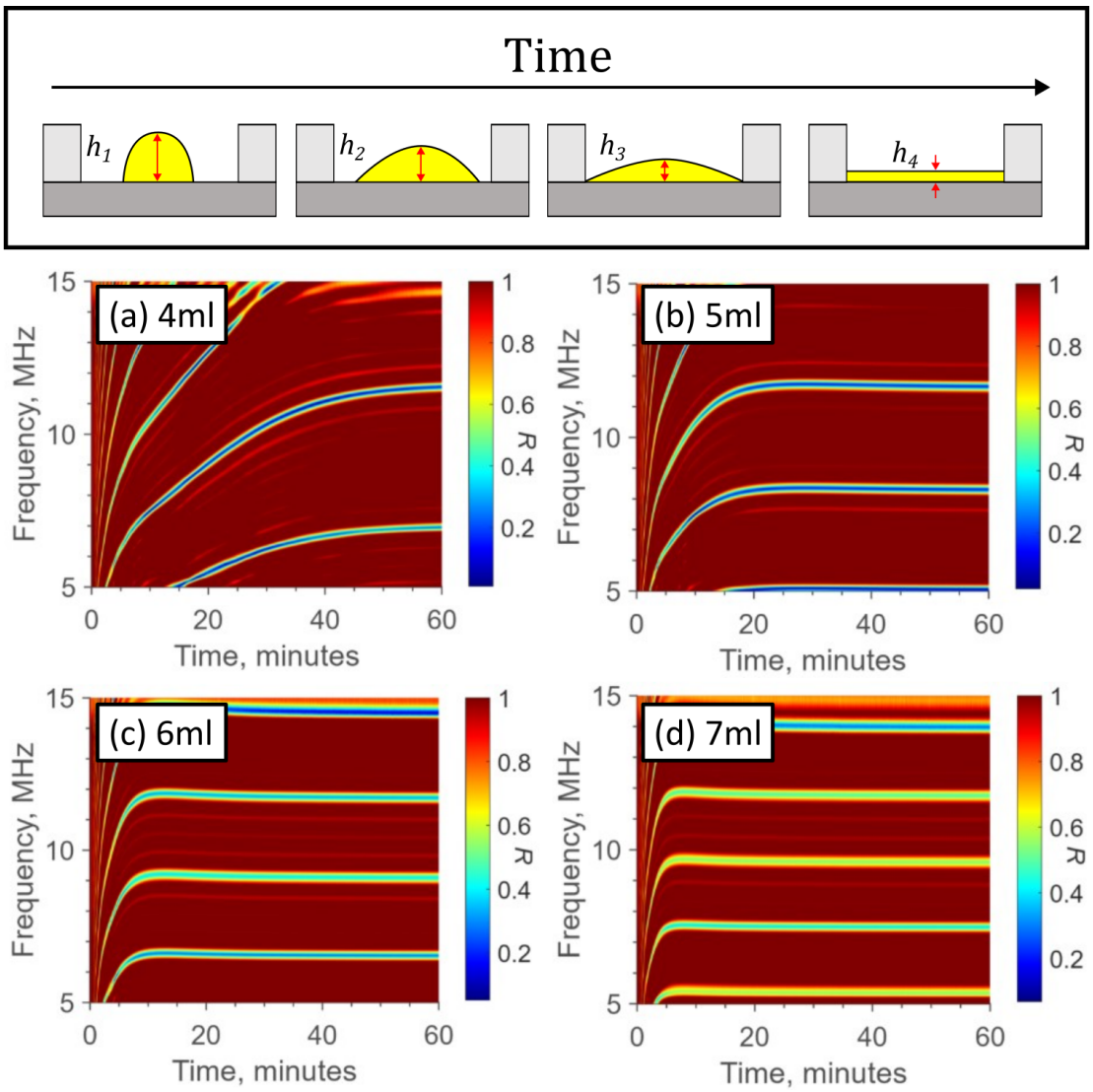

Figure 11: Spectral plots of 4ml, 5ml, 6ml and 7ml oil volumes deposited on the KOVOT test rig.

plotted in Fig. 6 as echo number is not considered and the wave is assumed continuos.

Fig. 12 shows the ultrasonically measured film thickness at the plate centre, calculated from the resonances shown in Fig. 11. Initially, there is a large scattering for all tests when the oil is first supplied as the film is thicker than the upper measurable limit via the resonance method. This then stops, and all tests show a clear reduction in the film thickness. As expected, the lower volume depositions formed thinner films, and take a longer time to stabilise. This is because the internal forces oppose the wetting action of the oil, whereas when the deposition is increased, these forces become somewhat irrelevant as the increased volume means the oil has more inertia and so spreads easier.

For each test, the stabilised film thickness was calculated/measured three ways; the theoretical height calculated from the deposited oil volume, the ultrasonically measured film thickness from six locations around the plate, and film comb measurements from five locations around the plate. Fig. 13 shows how the measurement techniques compare. The error bar for the volume method is calculated from the precision of calliper used to measure the internal diameter of the bath wall, and the precision of the syringe used to deposit the oil. The ultrasonic measurement and film comb measurement error bars are the standard deviation across the different locations. The fact that the ultrasonic method and film comb method have an error bar at all shows that the film formed was not perfectly level. Between ultrasonic measurements there was a maximum deviation of 11μm from the plate centre to an edge measurement. The film comb measured a maximum deviation of 50μm from the centre to edge, but the relatively low precision of the instrument makes this deviation understandable.

Across the four volumes tested, there is very good agreement between the mean film thickness measured via the ultrasonic method and film comb method. However, the theoretical deposited film, calculated from the bath wall dimensions, is larger than the other two methods, even

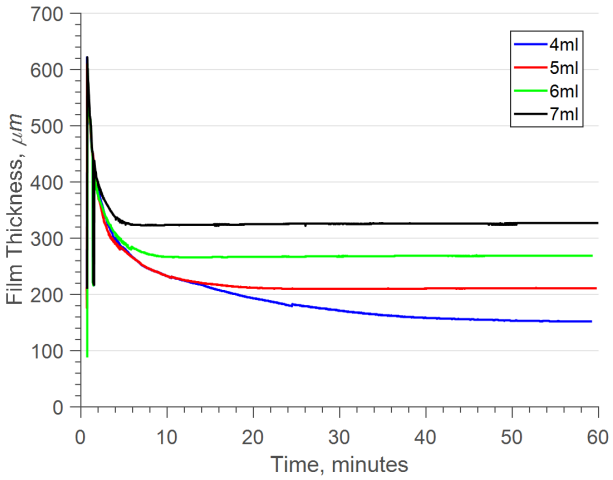

Figure 12: Ultrasonically measured central film thickness over a 60 minute duration with four different deposit volumes.

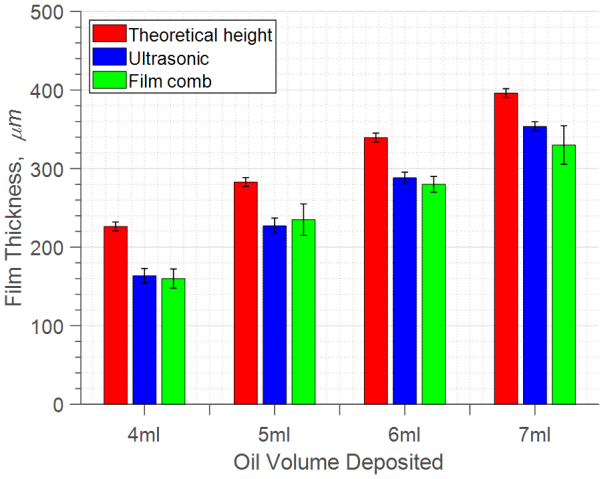

Figure 13: Comparison of the mean measured film thickness using ultrasonic sensor, film comb, and known volume deposition method.

when considering what the minimum film may be due to the deposition precision. The % difference between the mean ultrasonically measured film thickness and calculated film thickness from the oil volume is 32%, 22%, 16% and 11% from 4ml to 7ml respectively; that is to say, as the volume of oil increases the agreement between measurement techniques and the calculated volume improves.

The most rational explanation for this is a meniscus rim forming around the layer circumference, which wicks up the bath wall due to capillary action, making the deposited film formed thinner than the theoretical prediction. However, if the capillary action is independent on the volume of oil deposited, so long as there is ample oil to wick from, the % difference change would decrease with larger oil deposits, which is seen in the tests. If larger oil deposits were used then it is expected that agreement would improve, but the deposited layer would no longer be representative of a raceway film, and for this reason was not performed.

7 Measuring and Quantifying Raceway Thickness In-Situ

Ultrasonic reflections recorded from a raceway-oil film contact can be processed to calculate film thickness (48). Fig. 14 shows a visualisation of the raceway film at a single location along the rolling axis, as a single element passes over the sensor location. The film is around 400μm at both the inlet and outlet for this particular test case. Areas of scatter are highlighted in red showing an algorithm breakdown, due to an absence or instability of an oil film in the parched regions between contacts, where the reference reflections are taken. At the inlet, there is a small thickening up to the inlet meniscus position. At the contact exit, there is an outlet film, similar in thickness to the inlet but shorter, surviving only 20mm from the contact centre. Although this plot allows the visualisation of the raceway film, it is qualitative in nature, and only at a single sensor location, giving a limited benefit.

A moving variance method was developed to automate the detection of inlet and outlet films, thus allowing for the large-scale quantification of raceway film thickness. Fig. 15a shows a single inlet film divided into three regions of stability. The green region shows a clearly stable raceway film. The red region has large scatter suggesting there is no film present. In the yellow region there is some ambiguity about where the film forms and transitions to a stable one. To standardise the detection of the stable raceway film across roller passes, a moving standard variance window was used.

A window of a set number of reflections was selected; a trial and error approach deemed 20 reflections gave repeatable results. Fig. 15b shows an example plot of the moving variance window of the film in Fig. 15a. From analysing different roller patterns, a variance threshold of 2000 was deemed acceptable to define a stable raceway film. The acoustic velocity of a lubricant influences the precision of the thickness measurement, and therefore by extension the variance in films. As the acoustic velocities of all lubricants tested were very similar, a single threshold value could be used across all tests.

Once the variance value falls below this threshold, a stable film is assumed to be formed, and the mean is taken of all values after to determine the mean film thickness for that roller pass and sensor position. Before this value, the raceway film is too thin/non-present and the scatter values are ignored. This gives a single mean thickness value to represent the raceway lubrication condition at a single position along the rolling axis, allowing for film quantification.

Fig. 16a shows the mean raceway thickness up to around 10mm away from the contact centre, which is the limit of the measurement area, as shown by Fig. 14 and Fig. 15. The region closer to the contact is subjected to complex

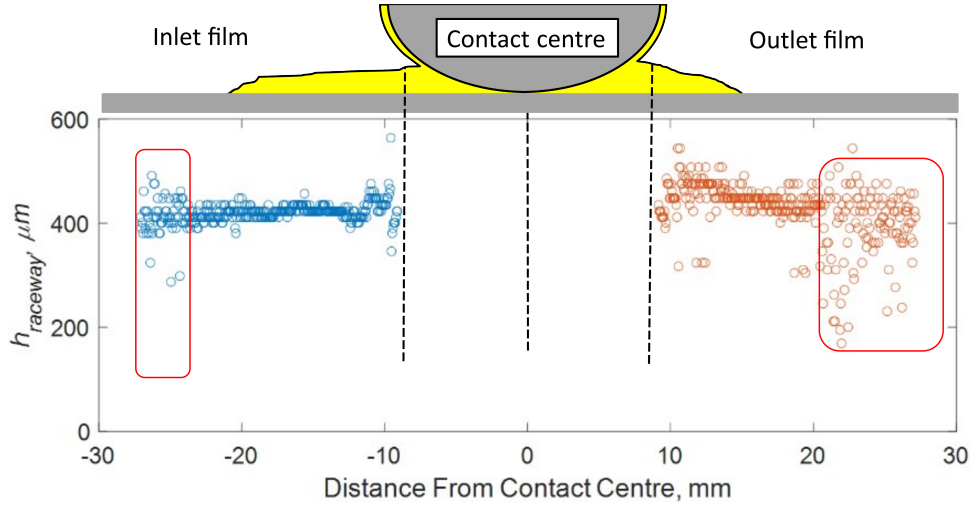

Figure 14: Visualisation of the raceway film at the contact inlet and outlet regions. Highlighted are regions of scatter where a stable film is not present.

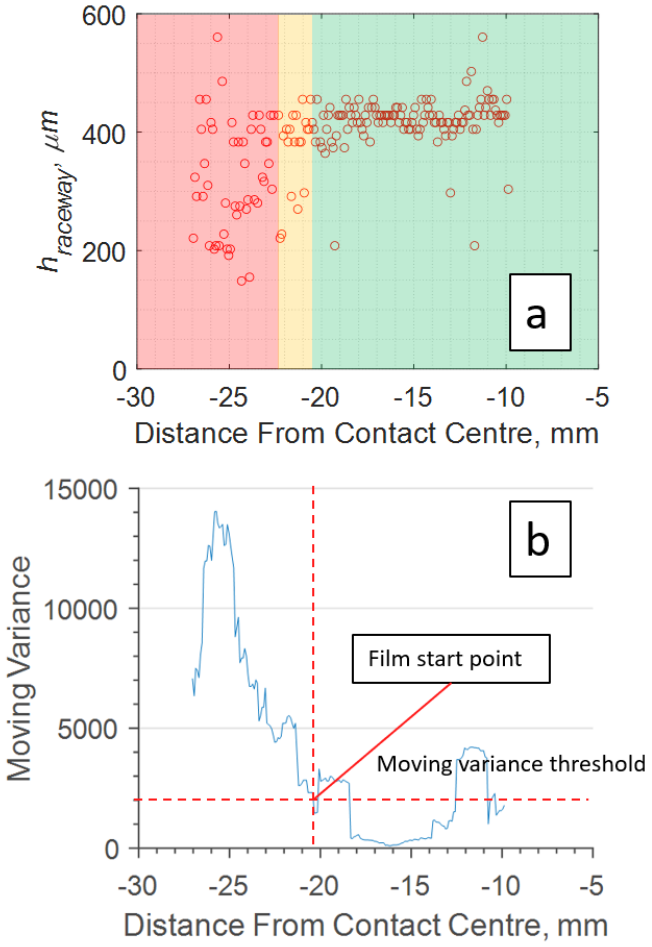

Figure 15: (a) shows the measured raceway film at the inlet to a contact with some scatter far away from the contact inlet. (b) shows the moving variance and determination of the raceway film detection area.

wave interference because of the convex roller and raceway geometries, making measurements in that region impossible. Fig. 16b is a schematic, as if looking head-on at a roller, to help visualise the film shape leading into the contact, and how this varies across the axis of a roller.

Although the bearing rollers do have crowning, the sensors central positions lie within the middle 66mm of the 82mm long roller, and so deviations from flat at the outer sensors are not considered. Error bars are standard error for the sensor at that axial location.

For this test case, both the VG320 and VG32 oils show thicker bands of oil towards the roller end faces, and a thinner film in the central region. The presence of oil bands and a depleted centre within the contact area have been observed both experimentally and theoretically for starved contacts (14, 15, 62), but this work shows that a 'U' shape distribution occurs under fully flooded conditions. This has many implications, such as churning losses not being equal across the rolling axis, and affects on roller skew, that must be explored in future work.

The more viscous VG320 forms a thicker film than the VG32 right across the rolling axis. The mean temperature was calculated from readings from the inner-raceway mounted thermocouple over the test capture, a duration of 10s. There is a deviation of just $0.43\,^{\circ}\mathrm{C}C$ between the tests using the two different oils at the same operating conditions. This then suggests the thicker inlet film developed by the VG320 oil is a direct result of its increased viscosity; most likely it has a stronger capillary effect and is therefore able to form thicker films easier.

8 Conclusions

This paper has presented the validation that oil films adhering to a bearing raceway are sensitive to ultrasonic resonance measurement techniques. Practical processing considerations such as signal duration, acoustic velocity and usable bandwidth have been discussed. The validation has been novelly applied to measure raceway films in-situ of

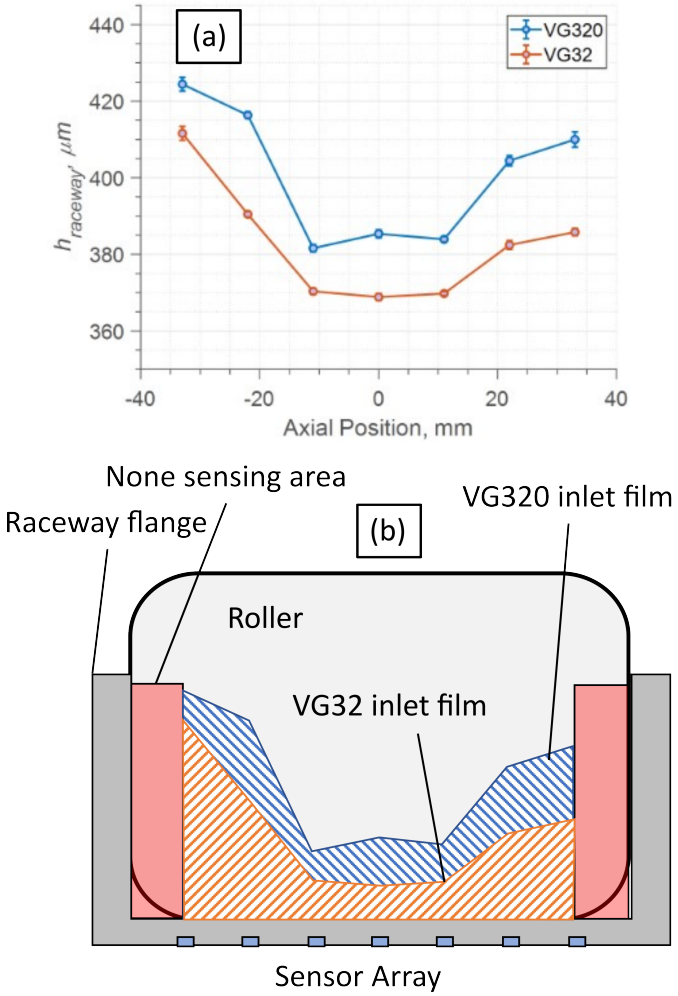

Figure 16: (a) Mean raceway thickness leading into the contact inlet at different axial locations when the bearing was lubricated with VG320 and VG32 oils. (b) shows a schematical representation of the results.

an operating, metallic rolling element bearing. The technique developed in this work will allow for new insights into rolling element bearing lubrication mechanisms, oil flow, and ultimately bearing health. Key conclusions and novelties are as follows:

- Oil films on bearing raceways are sensitive to ultrasonic resonances.
- Including more of the signal tail in analysis can increase the maximum film measurable, and measurement accuracy, of the resonance method.
- Defining a usable signal bandwidth is critical in eradicating false positive resonance readings. A conservative −6db is recommended for bearing applications.
- Ideally, multiple resonances should be recorded and f_0 calculated from the frequency difference. If this is not possible, a set of three rules are proposed to ensure a single resonance is f_0 and not a higher order harmonic.
- A moving variance method has been developed to quantify large raceway oil film data into a comparable, mean thickness value.

Author Contributions

WG performed the experiments, completed the data analysis and wrote the first draft of the manuscript. RDJ provided expert guidance during the course of the work. All authors contributed towards manuscript revision, and approved the final submitted manuscript.

Funding

The authors would like to acknowledge the financial support of the Timken Company who co-funded this work, and would also like to acknowledge the Engineering and Physical Sciences Research Council for funding through RDJ's fellowship on Tribo-Acoustic Sensors EP/N016483/1 and the Centre for Doctoral Training in Integrated Tribology EP/L01629X/1. For the purpose of open access, the author has applied a Creative Commons Attribution (CC BY) licence to any Author Accepted Manuscript version arising.

Acknowledgements

The authors would like to acknowledge the help and advice of Dr Bill Hannon of The Timken Co. for his guidance throughout the work.

References

[1] J. A. Williams, Engineering Tribology, Cambridge University Press, 2005.

[2] H. A. Spikes, Sixty years of EHL, Lubr. Sci. 18 (4) (2006) 265–291. doi:10.1002/ls.23.

[3] R. Kumar, M. S. Azam, S. K. Ghosh, S. Yadav, 70 years of Elastohydrodynamic Lubrication (EHL): A Review on Experimental Techniques for Film Thickness and Pressure Measurement, Mapan - J. Metrol. Soc. India 33 (4) (2018) 481–491. doi:10.1007/s12647-018-0277-1.

[4] D. Dowson, G. R. Higginson, A Numerical Solution to the Elasto-Hydrodynamic Problem, J. Mech. Eng. Sci. 1 (1) (1959) 6–15. doi:10.1243/JMES_JOUR_1959_001_004_02.
URL http://journals.sagepub.com/doi/10.1243/JMES{_}JOUR{_}1959{_}001{_}004{_}02

[5] D. Dowson, G. R. Higginson, The Effect of Material Properties on the Lubrication of Elastic Rollers, J. Mech. Eng. Sci. 2 (3) (1960) 188–194. doi:10.1243/jmes_jour_1960_002_028_02.

[6] D. Dowson, G. R. Higginson, New Roller-Bearing Lubrication Formula, Tech. rep. (1961).

[7] D. Dowson, G. R. Higginson, A. V. Whitaker, Elasto-Hydrodynamic Lubrication: A Survey of Isothermal Solutions, J. Mech. Eng. Sci. 4 (2) (1962) 121–126. doi:10.1243/jmes_jour_1962_004_018_02.

[8] D. Dowson, Paper R1: Elastohydrodynamic Lubrication: An Introduction and a Rexview of Theoretical Studies, Proc. Inst. Mech. Eng. Conf. Proc. 180 (2) (1965) 7–16. doi:10.1243/pime_conf_1965_180_059_02.

[9] D. Dowson, The inlet boundary condition (1974) 143–152.

[10] D. Dowson, A. Toyoda, A central film thickness formula for ehd line contacts, in: Proc. 5th Leeds-Lyon Symp., Mechanical Engineering Publications, London, 1978.

[11] A. W. Crook, The Lubrication of Rollers., in: Philos. Trans. R. Soc. London, Vol. 250, 1958, pp. 387–409. URL https://www.jstor.org/stable/pdf/91607.pdf?refreqid=excelsior{%}3A185349e4ba513dff50cc43f525a2786c{&}ab{_}segments={&}origin={&}acceptTC=1

[12] A. W. Crook, The Lubrication of Rollers II . Film Thickness with Relation to Viscosity and Speed, Philos. Trans. R. Soc. London 254 (1040) (1961) 223–236.

[13] L. D. Wedeven, D. Evans, A. Cameron, Optical Analysis of Ball Bearing Starvation, J. Lubr. Technol. 93 (3) (1971) 349. doi:10.1115/1.3451591.
URL https://asmedigitalcollection.asme.org/tribology/article/93/3/349/417808/Optical-Analysis-of-Ball-Bearing-Starvation

[14] F. Chevalier, A. A. Lubrecht, P. M. Cann, F. Colin, G. Dalmaz, Film thickness in starved EHL point contacts, J. Tribol. 120 (1) (1998) 126–133. doi:10.1115/1.2834175.

[15] H. Chen, W. Wang, H. Liang, X. Ge, Observation of the oil flow in a ball bearing with a novel experiment method and simulation, Tribol. Int. 174 (June) (2022) 107731. doi:10.1016/j.triboint.2022.107731.
URL https://doi.org/10.1016/j.triboint.2022.107731

[16] M. Chennaoui, M. Fowell, H. Liang, A. Kadiric, A Novel Set-Up for In Situ Measurement and Mapping of Lubricant Film Thickness in a Model Rolling Bearing Using Interferometry and Ratiometric Fluorescence Imaging, Tribol. Lett. 70 (3) (2022) 1–17. doi:10.1007/s11249-022-01625-z.
URL https://doi.org/10.1007/s11249-022-01625-z

[17] P. M. Lugt, A review on grease lubrication in rolling bearings, Tribol. Trans. 52 (4) (2009) 470–480. doi:10.1080/10402000802687940.

[18] P. M. Lugt, Grease Lubrication In Rolling Bearings, John Wiley & Sons, Ltd, 2013. doi:10.1201/b19033-24.

[19] V. Bruyere, N. Fillot, G. E. Morales-Espejel, P. Vergne, A two-phase flow approach for the outlet of lubricated line contacts, J. Tribol. 134 (4) (2012) 1–10. doi:10.1115/1.4006277.

[20] D. Koštál, D. Nečas, P. Šperka, P. Svoboda, I. Křupka, M. Hartl, Lubricant Rupture Ratio at Elastohydrodynamically Lubricated Contact Outlet, Tribol. Lett. 59 (3) (2015) 1–9. doi:10.1007/s11249-015-0565-7.

[21] B. Damiens, C. H. Venner, P. M. E. Cann, A. A. Lubrecht, Starved lubrication of elliptical EHD contacts, J. Tribol. 126 (1) (2004) 105–111. doi:10.1115/1.1631020.

[22] H. G. Elrod, A cavitation algorithm., Trans. ASME 103 (July) (1980).

[23] H. Moes, Lubrication and Beyond, Twente University Press, Twente, 2000.

[24] P. M. E. Cann, B. Damiens, A. A. Lubrecht, The transition between fully flooded and starved regimes in EHL, Tribol. Int. 37 (10) (2004) 859–864. doi:10.1016/j.triboint.2004.05.005.

[25] M. T. van Zoelen, C. H. Venner, P. M. Lugt, Prediction of film thickness decay in starved elastohydrodynamically lubricated contacts using a thin layer flow model, Proc. Inst. Mech. Eng. Part J J. Eng. Tribol. 223 (3) (2009) 541–552. doi:10.1243/13506501JET524.

[26] P. Svoboda, D. Kostal, I. Krupka, M. Hartl, Experimental study of starved EHL contacts based on thickness of oil layer in the contact inlet, Tribol. Int. 67 (2013) 140–145. doi:10.1016/j.triboint.2013.07.019.
URL http://dx.doi.org/10.1016/j.triboint.2013.07.019

[27] D. Kostal, P. Sperka, P. Svoboda, I. Krupka, M. Hartl, Influence of Lubricant Inlet Film Thickness on Elastohydrodynamically Lubricated Contact Starvation, J. Tribol. 139 (5) (2017) 1–6. doi:10.1115/1.4035777.

[28] M. T. van Zoelen, C. H. Venner, P. M. Lugt, Free surface thin layer flow on bearing raceways, J. Tribol. 130 (2) (2008) 1–10. doi:10.1115/1.2805433.

[29] P. Shetty, R. J. Meijer, J. A. Osara, P. M. Lugt, Measuring Film Thickness in Starved Grease-Lubricated

Ball Bearings: An Improved Electrical Capacitance Method, Tribol. Trans. 65 (5) (2022) 869–879. doi:10.1080/10402004.2022.2091067.
URL https://doi.org/10.1080/10402004.2022.2091067

[30] R. S. Dwyer-Joyce, B. W. Drinkwater, C. J. Donohoe, The measurement of lubricant- Film thickness using ultrasound, Proc. R. Soc. A Math. Phys. Eng. Sci. 459 (2032) (2003) 957–976. doi:10.1098/rspa.2002.1018The.

[31] P. Dou, Y. Jia, P. Zheng, T. Wu, M. Yu, T. Reddyhoff, Z. Peng, Review of ultrasonic-based technology for oil film thickness measurement in lubrication, Tribol. Int. 165 (August 2021) (2022) 107290. doi:10.1016/j.triboint.2021.107290.
URL https://doi.org/10.1016/j.triboint.2021.107290

[32] M. Schirru, M. Varga, Tribology Letters A review of ultrasonic reflectometry for the physical characterization of lubricated tribological contacts : history , methods , devices , and technological trends, Tribol. Lett. (2022) 1–22doi:10.1007/s11249-022-01670-8.
URL https://doi.org/10.1007/s11249-022-01670-8

[33] T. Howard, Development of a Novel Bearing Concept for Improved Wind Turbine Gearbox Reliability, Phd thesis, University of Sheffield (2016).

[34] G. Nicholas, Development of Novel Ultrasonic Monitoring Techniques for Improving the Reliability of Wind Turbine Gearboxes, Phd thesis, University of Sheffield (2021).

[35] N. F. Haines, J. C. Bell, P. J. McIntyre, The application of broadband ultrasonic spectroscopy to the study of layered media, J. Acoust. Soc. Am. 64 (6) (1978) 1645–1651. doi:10.1121/1.382131.

[36] T. Pialucha, C. C. H. Guyott, P. Cawley, Amplitude spectrum method for the measurement of phase velocity, Ultrasonics 27 (5) (1989) 270–279. doi:10.1016/0041-624X(89)90068-1.

[37] T. Pialucha, P. Cawley, The detection of thin embedded layers using normal incidence ultrasound, Ultrasonics 32 (6) (1994) 431–440. doi:10.1016/0041-624X(94)90062-0.

[38] H. Tohmyoh, M. Suzuki, Measurement of the coating thickness on the back side of double-sided coated structures by means of acoustic resonant spectroscopy, Surf. Coatings Technol. 204 (4) (2009) 546–550. doi:10.1016/j.surfcoat.2009.08.040.
URL http://dx.doi.org/10.1016/j.surfcoat.2009.08.040

[39] H. Tohmyoh, T. Sunaga, M. Suzuki, Simultaneous observation of acoustic resonance phenomena at both surfaces of a plate coated with thin layers, Rev. Sci. Instrum. 83 (3) (2012). doi:10.1063/1.3698088.

[40] T. Sunaga, H. Tohmyoh, M. Suzuki, Characterization of polymer thin coating on substrate by acoustic resonant spectroscopy, Thin Solid Films 544 (2013) 437–442. doi:10.1016/j.tsf.2013.02.085.
URL http://dx.doi.org/10.1016/j.tsf.2013.02.085

[41] R. S. Dwyer-Joyce, P. Harper, B. W. Drinkwater, A method for the measurement of hydrodynamic oil films using ultrasonic reflection, Tribol. Lett. 17 (2) (2004) 337–348. doi:10.1023/B:TRIL.0000032472.64419.1f.

[42] S. Beamish, R. S. Dwyer-Joyce, Measuring Oil Films in Dynamically Loaded Journal Bearings via the Ultrasonic Technique (2015).

[43] S. Beamish, Oil Film Thickness Measurements in Journal Bearings under Normal , Severe & Dynamic Loading Conditions using Ultrasound, Ph.D. thesis, The University of Sheffield (2021).

[44] S. Beamish, R. S. Dwyer-Joyce, Experimental Measurements of Oil Films in a Dynamically Loaded Journal Bearing, Tribol. Trans. 65 (6) (2022) 1022–1040. doi:10.1080/10402004.2022.2106926.
URL https://doi.org/10.1080/10402004.2022.2106926

[45] P. C. Pedersen, Z. Cakareski, J. C. Hermanson, Ultrasonic monitoring of film condensation for applications in reduced gravity, Ultrasonics 38 (1) (2000) 486–490. doi:10.1016/S0041-624X(99)00214-0.

[46] Z. Q. Chen, J. C. Hermanson, M. A. Shear, P. C. Pedersen, Ultrasonic monitoring of interfacial motion of condensing and non-condensing liquid films, Flow Meas. Instrum. 16 (6) (2005) 353–364. doi:10.1016/j.flowmeasinst.2005.06.002.

[47] J. Kanja, R. Mills, X. Li, H. Brunskill, A. K. Hunter, R. S. Dwyer-Joyce, Non-contact measurement of the thickness of a surface film using a superimposed ultrasonic standing wave, Ultrasonics 110 (2021). doi:10.1016/j.ultras.2020.106291.

[48] W. A. Gray, R. S. Dwyer-Joyce, In-situ measurement of the meniscus at the entry and exit of grease and oil lubricated rolling bearing contacts, Front. Mech. Eng. 8 (2032) (2022) 2032. doi:10.3389/fmech.2022.1056950.
URL https://www.frontiersin.org/articles/10.3389/fmech.2022.1056950/full

[49] W. A. Gray, In-Situ Measurement of the Roller Bearing Inlet Meniscus Using Ultrasonic Spectroscopy, Ph.D. thesis, University of Sheffield (2024).
URL https://etheses.whiterose.ac.uk/35144/

[50] L. E. Kinsler, A. R. Frey, A. B. Coppens, S. V. Sanders, Fundamentals of Acoustics, John Wiley & Sons, Incorporated, 2000.

[51] L. M. Brekhovskikh, Waves in layered media, Academic Press, New York ; London, 1960.

[52] T. E. G. Alvarez-Arenas, Acoustic Impedance Matching of Piezoelectric, IEEE Trans. Ultrason. Ferroelectr. Freq. Control 51 (5) (2004) 624–633.

[53] M. Schirru, R. Mills, R. S. Dwyer-Joyce, O. Smith, M. Sutton, Viscosity Measurement in a Lubricant Film Using an Ultrasonically Resonating Matching Layer, Tribol. Lett. 60 (3) (2015) 1–11. doi:10.1007/s11249-015-0619-x.

[54] D. M. Egle, D. E. Bray, Measurement of acoustoelastic and third-order elastic constants for rail steel, J. Acoust. Soc. Am. 60 (3) (1976) 741–744. doi:10.1121/1.381146.

[55] G. Nicholas, B. P. Clarke, R. S. Dwyer-Joyce, Detection of Lubrication State in a Field Operational Wind Turbine Gearbox Bearing Using Ultrasonic Reflectometry, Lubricants 9 (1) (2021) 6. doi:10.3390/lubricants9010006.
URL https://www.mdpi.com/2075-4442/9/1/6

[56] P. A. Oliveira, R. M. B. Silva, G. C. Morais, A. V. Alvarenga, R. P. B. Costa-Félix, Speed of sound as a function of temperature for ultrasonic propagation in soybean oil, J. Phys. Conf. Ser. 733 (1) (2016). doi:10.1088/1742-6596/733/1/012040.

[57] N. A. Azman, S. B. Abd Hamid, Determining the Time of Flight and Speed of Sound on Different types of Edible Oil, IOP Conf. Ser. Mater. Sci. Eng. 260 (1) (2017) 0–6. doi:10.1088/1757-899X/260/1/012034.

[58] N. Bilaniuk, G. S. K. Wong, Speed of sound in pure water as a function of temperature, J. Acoust. Soc. Am. 93 (3) (1993) 1609–1612. doi:10.1121/1.406819.

[59] W. Marczak, Water as a standard in the measurements of speed of sound in liquids, J. Acoust. Soc. Am. 102 (5) (1997) 2776–2779. doi:10.1121/1.420332.

[60] P. Dou, T. Wu, Z. Luo, Z. Peng, T. Sarkodie-Gyan, The application of the principle of wave superposition in ultrasonic measurement of lubricant film thickness, Meas. J. Int. Meas. Confed. 137 (2019) 312–322. doi:10.1016/j.measurement.2019.01.057.
URL https://doi.org/10.1016/j.measurement.2019.01.057

[61] S. Kihong, J. K. Hammond, Fundamentals Of Signal Tracking Theory, John Wiley & Sons, Ltd, 1996. doi:10.2514/5.9781600866388.0245.0327.

[62] F. Chevalier, A. A. Lubrecht, P. M. E. Cann, F. Colin, G. Dalmaz, Starved Film Thickness: a Qualitative Explanation, in: D. Dowson, C. M. Taylor, T. H. C. Childs, G. Dalmaz (Eds.), Lubr. Lubr., Vol. 30 of Tribology Series, Elsevier, 1994, pp. 249–257. doi:https://doi.org/10.1016/S0167-8922(08)70634-5.
URL https://www.sciencedirect.com/science/article/pii/S0167892208706345